

DUSTY WIND-BLOWN BUBBLES

BY J.E. EVERETT^{1,2,3}, E. CHURCHWELL¹

Accepted to ApJ

ABSTRACT

Spurred by recent observations of $24\mu\text{m}$ emission within wind-blown bubbles, we study the role that dust can play in such environments, and build an approximate model of a particular wind-blown bubble, ‘N49.’ First, we model the observations with a dusty wind-blown bubble, and then ask whether dust could survive within N49 to its present age (estimated to be 5×10^5 to 10^6 years). We find that dust sputtering and especially dust-gas friction would imply relatively short timescales ($t \sim 10^4$ years) for dust survival in the wind-shocked region of the bubble. To explain the $24\mu\text{m}$ emission, we postulate that the grains are replenished within the wind-blown bubble by destruction of embedded, dense cloudlets of ISM gas that have been over-run by the expanding wind-blown bubble. We calculate the ablation timescales for cloudlets within N49 and find approximate parameters for the embedded cloudlets that can replenish the dust; the parameters for the cloudlets are roughly similar to those observed in other nebula. Such dust will have an important effect on the bubble: including simple dust cooling in a wind-blown bubble model for N49, we find that the luminosity is higher by approximately a factor of six at a bubble age of about 10^4 years. At ages of 10^7 years, the energy contained in the bubble is lower by about a factor of eight if dust is included; if dust must be replenished within the bubble, the associated accompanying gas mass will also be very important to wind-blown bubble cooling and evolution. While more detailed models are certainly called for, this work illustrates the possible strong importance of dust in wind-blown bubbles, and is a first step toward models of dusty, wind-blown bubbles.

Subject headings: ISM:bubbles, dust, stars:individual (N49)

1. INTRODUCTION

In addition to the energy, mass, and momentum input provided by the deaths of massive stars in supernovae, early-type stars also launch hypersonic ($v \sim 1000\text{--}3000\text{ km s}^{-1}$, whereas $c_{s,\text{ISM}} \sim 10\text{ km s}^{-1}$) winds with mass outflow rates of order 10^{-7} to $10^{-6} M_{\odot} \text{ yr}^{-1}$ (although clumping within the wind may imply smaller mass-outflow rates; see Hillier 2009). Such winds drive forward shocks both into the surrounding interstellar medium and reverse shocks back into the stellar wind; these reverse shocks then heat the stellar wind into a pressurized bubble surrounding the young star, resulting in objects known as wind-blown bubbles (WBBs; for reviews see, e.g., Zhekov & Myasnikov 2000; Chu 2003; Arthur 2007; Chu 2008). WBBs are therefore thought to have four major components: (1) an inner, free-flowing, hypersonic wind surrounded by (2) the hot, post-shocked wind plasma, which is enclosed by (3) a thin shell of 10^4 K gas which resides in (4) the ambient interstellar medium (see Figure 1 of Weaver et al. 1977, for a sketch of these components; they also form the basis of our Fig. 14).

The structure of these WBBs is useful to study in that they help us understand the transformation of gas phases in the interstellar medium, and more generally, the impact of massive stars on their host molecular clouds, the heating of ISM gas, and the input of energy into turbulence in the ISM (e.g., Hensler 2008); they may even trigger star formation on their periphery (Churchwell et al. 2006). Observations of WBBs also place constraints on stellar-wind power over the evolution of early-type stars. Finally, WBBs are important for set-

ting the stage for the star’s subsequent supernova explosion or perhaps gamma-ray burst.

These wind-blown bubbles and their impact on the interstellar medium have been observed for many years (e.g., Johnson & Hogg 1965; Smith 1967; Chu & Lasker 1980; Nazé et al. 2001; Churchwell et al. 2006; Watson et al. 2008). Theoretical work in understanding these observations has been pursued in parallel by many researchers (e.g., Johnson & Hogg 1965; Mathews 1966; Pikel’ner 1968; Dyson 1973; Castor et al. 1975; Falle 1975; Weaver et al. 1977; Hartquist et al. 1986; Arthur et al. 1993; Garcia-Segura & Mac Low 1995; Garcia-Segura et al. 1996; Arthur et al. 1996; Pittard et al. 2001a,b; Nazé et al. 2002; Freyer et al. 2003, 2006). These dynamical studies of wind-blown bubbles have included detailed modelling of the effect of a surrounding inhomogeneous medium (and especially, the role of clumps in the surrounding medium, which will become important later in this work; see Arthur et al. 1993; Pittard et al. 2001b; Nazé et al. 2002, for example). To the present day, however, such models have not included the role of dust. Recent observations by Churchwell et al. (2006) and Watson et al. (2008) present evidence that dust exists within WBBs. What role does this dust play in the structure and the evolution of the bubbles, and how might dust modify the impact of WBBs on the surrounding interstellar medium?

This paper aims to study the role of dust in wind-blown bubbles in the context of observations of one WBB: N49. We will start by briefly outlining the observations of N49 in Section 2. This paper will then examine the role of dust within N49; in particular, we ask if dust can explain the observed $24\mu\text{m}$ emission around N49 (examined in Section 3), and then ask if dust can survive within the $10^6\text{--}10^7\text{ K}$, post-shocked wind-blown bubble in N49 in Section 4. Then, in Section 5, we offer a simple model to explain the observations and our results on dust survival. Our conclusions are presented in Section 6.

everett@physics.wisc.edu

¹ University of Wisconsin–Madison, Department of Astronomy

² University of Wisconsin–Madison, Department of Physics

³ Center for Magnetic Self-Organization in Laboratory and Astrophysical Plasmas

2. OBSERVED MID-IR CONTINUUM DISTRIBUTION

This paper considers the mid-infrared signature of one particular WBB: ‘N49.’ N49 was discovered in the infrared and cataloged by Churchwell et al. (2006) as part of a manual search of the Galactic Legacy Infrared Mid-Plane Survey Extraordinaire (GLIMPSE; see Benjamin et al. 2003; Churchwell et al. 2009) taken by the *Spitzer Space Telescope* (Werner et al. 2004). Churchwell et al. (2006) found over 300 partial and closed rings in their search of the GLIMPSE data; their paper presents an analysis of the characteristics of the (incomplete) large population of bubbles reported. A later catalog for bubbles within $|l| < 10^\circ$ in the Galaxy found a comparable number. These bubbles were identified by rings of $8\mu\text{m}$ emission that were found to enclose $24\mu\text{m}$ emission; a few such infrared bubbles had been detected before by the *Infrared Space Observatory* and by the *Midcourse Space Experiment* (e.g., Pasquali et al. 2002; Deharveng et al. 2005; Vasquez et al. 2009).

N49 was later the focus of a more detailed study by Watson et al. (2008). For that study, N49 was chosen because of its relatively symmetric appearance: for instance, the $8\mu\text{m}$ emission was very well fit by assuming a spherical shell (see Fig. 12 of Watson et al. 2008). This implies that perhaps N49 is a useful test case for comparing with models of WBB evolution. Watson et al. (2008) also examined $24\mu\text{m}$ emission observed with the Multiband Imaging Photometer aboard *Spitzer* (MIPS; Rieke et al. 2004) as part of the the MIPS Galactic Plane Survey (MIPSGAL; see Carey et al. 2009), comparing that data to $8\mu\text{m}$ *Spitzer* observations and to 20 cm radio observations (Helfand et al. 2006). These data showed that emission at $24\mu\text{m}$ and 20 cm are coincident, sharing the same annular geometry (although the 20 cm data, indicating free-free emission from ionized gas, does not drop off quite as quickly with radius as the $24\mu\text{m}$ emission); both were also enclosed by the larger-radius $8\mu\text{m}$ emission of the photodissociation region (PDR) shell, strongly indicating that the dusty post-shocked gas resides within the outlying $8\mu\text{m}$ PDR shell. However, it is not at all clear if a reasonable mass of dust could explain the observed emission, and if dust could survive in that post-shocked gas environment. And, if dust can exist within the bubble, what role might such dust play in the evolution of wind-blown bubbles? These are the questions that the present paper sets out to answer.

3. MODELLING THE MID-IR CONTINUUM DISTRIBUTION

Our first task was to see whether dust emission (alone) is a reasonable fit to the observations. To synthesize observations of dust in WBBs, we have run photoionization simulations using ‘Cloudy’ (version 07.02.01, last described by Ferland et al. 1998). In those Cloudy simulations, we investigated emission from a constant-temperature ISM plasma with an included ‘normal’ dust grain population (using the dust-grain size distribution of Mathis et al. 1977) with a dust-mass-to-gas-mass ratio of 6.4×10^{-3} . We employed Cloudy_3D (Morisset 2006) to map the 1D Cloudy simulations into a spherically-symmetric 3D bubble that was then projected onto the plane of the sky to compare with observations. Note that Cloudy cannot model the dynamic post-shock structure of the WBB, so for photoionization studies, we model the impact of dusty gas on a *static* bubble of uniform temperature which we set. At this early stage, we have no dynamical model of dust fluxes into, or out of, the bubble; we are examining the emission from a dusty ISM plasma within the bubble, with a

standard ISM dust-to-gas ratio.

The parameters for the simulations and analysis are summarized in Table 1, along with references for the values used. We describe and justify those parameter choices in the paragraphs that follow.

Parameter	Value	Reference
central star	O5V	Watson et al. (2008)
\dot{M}_{wind}	$1.5 \times 10^{-6} M_{\odot} \text{ yr}^{-1}$	Vink et al. (2001)
distance	5.7 kpc	Churchwell et al. (2006)
age	$\sim 10^6$ yrs	Watson et al. (2008)
$\langle n_{\text{inner, dusty gas}} \rangle$	19.1 cm^{-3}	(Best-Fit, $24\mu\text{m}$ data)
gas & dust density power law: r^α	$\alpha = -2$	Assumed
r_{inner}	0.6 pc	(Best-Fit, $24\mu\text{m}$ data)
r_{outer}	2.2 pc	interface of PDR shell
dust	ISM grain distribution	Mathis et al. (1977) van Hoof et al. (2004)
$T_{\text{e,bubble}}$	3.5×10^6 K	Our dynamical model (Section 4.2)

Table 1

The values used for parameters in the Cloudy simulations of the dusty wind-blown bubble, N49.

For the central star and its central stellar continuum, we include a star of class O5V (Watson et al. 2008). Using Cloudy’s ‘wmbasic’ stellar continuum models (Pauldrach et al. 2001, which include line-blanketing by stellar winds), and calling on the models in Table 1 of Martins et al. (2005), we set the star’s luminosity to $10^{5.51} L_{\odot}$, the surface temperature to $T_{\text{eff}} = 41540$ K, the surface gravity to $\log(g) = 3.92$, and the star’s metallicity to solar. These parameters correspond to a $37.3 M_{\odot}$ star, with a flux of hydrogen-ionizing photons of $\log q_0 = 10^{24.4}$ photons $\text{cm}^{-2} \text{ s}^{-1}$ or $\log Q_0 = 10^{49.3}$ photons s^{-1} into 4π steradians, very close to the value cited by Watson et al. (2008).

The stellar mass loss rate, \dot{M}_{wind} is not used directly in the Cloudy simulations, but used in our analysis of the velocity of the post-shocked gas to estimate (later) the dust-gas friction that drags dust out of the post-shocked wind region. For the stellar parameters we’ve adopted, the IDL code ‘Mdot.pro’ from Vink et al. (2001) yields a mass outflow rate of $1.4 \times 10^{-6} M_{\odot} \text{ yr}^{-1}$ and $v_{\infty} \sim 2600$ km s^{-1} . This yields a wind kinetic luminosity of 3×10^{36} ergs s^{-1} .

The kinematic distance to N49 is 5.7 ± 0.6 kpc (Churchwell et al. 2006). Given this distance, the size of the bubble, r_{outer} , is set by the inner radius of PAH emission, so is observationally estimated (Watson et al. 2008) as 2.2 pc. The density of ambient gas surrounding N49 is not well constrained, but unpublished observations of NH_3 emission (Cyganowski et al., in preparation) surrounding N49 indicate a high ambient gas density of order 10^4 cm^{-3} . The age of N49 is not well constrained, but if the external medium has a gas density of order 10^4 cm^{-3} , the age of a wind-blown bubble of the inferred size for N49 is approximately 5×10^5 to 10^6 years (Watson et al. 2008).

Again, since Cloudy does not simulate the heating of the wind’s post-shocked gas, we start by modelling the WBB with a uniform temperature for the post-shocked gas. For most of the simulations, we have chosen 3.5×10^6 K as that constant temperature; this value for the temperature is informed by our own simple dynamical models of wind-blown bubble

dynamics with dust cooling (see Section 4.2). Changes in the WBB temperature affect the amount of dust that is inferred; increasing the temperature to 10^7 K as suggested in the dust-free models of Freyer et al. (2003) would reduce the amount of dust required, but not eliminate it.

Finally, we assume that the grain distribution, which we specify in *Cloudy*, is an ISM-type grain distribution (Mathis et al. 1977; van Hoof et al. 2004). We explain below, in Section 3.1 why that grain distribution seems to be preferred by the observations.

3.1. Fitting $24\ \mu\text{m}$ observations with *Cloudy* models

First, we ask whether dust emission can reproduce the *Spitzer* $24\ \mu\text{m}$ observations of N49. Using the above-defined *Cloudy* and *Cloudy_3D* models, we simulate the emission in the *Spitzer* MIPS $24\ \mu\text{m}$ band⁴ by defining a filter centered on $23.7\ \mu\text{m}$ that spans from $21.65\ \mu\text{m}$ to $26.35\ \mu\text{m}$; we also define, for later use, the MIPS $70\ \mu\text{m}$ band, centered on $71.0\ \mu\text{m}$, spanning wavelengths from $61.5\ \mu\text{m}$ to $80.5\ \mu\text{m}$. To compare to the data, we take azimuthal averages of both the *Spitzer* data (Churchwell et al. 2006; Watson et al. 2008) and the photoionization model. For the *Spitzer* MIPS data, we take the flux average over 50 concentric annuli that have a Δr of 2 pixels (with one pixel = $1.25''$), centered on the centroid of flux within the bubble; the result of this azimuthal averaging is shown by the solid line in Figure 1. The background emission is estimated by calculating the average flux in an annulus with an inner radius of 130 pixels from the bubble centroid, and an outer radius of 150 pixels from the bubble centroid, where there are no background stars. The 1σ variance in the per-pixel flux is shown by the error bars in the figure; plotting this variance helps to confirm that the rise (at about $25''$) and fall of the $24\ \mu\text{m}$ emission is present, but with some variations that we have averaged out.

We first performed a large-scale, manual search of parameter space for the approximate gas density and the approximate WBB inner radius that reproduced the observations; we started our search at $n = 1\ \text{cm}^{-3}$ and $r_{\text{inner}} = 0.5\ \text{pc}$ (the last value is taken from the approximate observed inner radius of $24\ \mu\text{m}$ dust emission). After manually increasing the gas density, n , to reproduce approximately the observed dust emission, we then set up an automated grid search of the parameter space stretching from $\log(r_{\text{inner}}/\text{cm}) = 18.15$ to 18.30 in steps of 0.05, and with $\langle n_{\text{dusty gas}}(r_{\text{inner}}) \rangle = 19.00$ to $21.00\ \text{cm}^{-3}$ in steps of 0.25, followed by higher-resolution searches with step-sizes down to 0.01 in $\log(r_{\text{inner}})$ and 0.0625 in $\langle n_{\text{dusty gas}}(r_{\text{inner}}) \rangle$. This allowed much more accurate estimates of the WBB parameters. In all of our parameter searches, there was no apparent degeneracy in χ^2 for the two parameters investigated, and only one minimum in χ^2 was found, producing a unique fit to the data (we used Poisson errors in calculating χ^2 , weighting the large-scale radial decline in $24\ \mu\text{m}$ emission with radius, and not the central depression in emission).

We find a reasonable match to the $24\ \mu\text{m}$ emission, as shown by the dashed line in Figure 1. For this fit, we specify that the dusty gas density scales as $n(r) \propto r^{-2}$ and find the best-fit initial density and inner radius (again, see Table 1 for input parameters and resultant best-fit parameters). This particular power-law for the density was chosen because it fit the observed pattern of $24\ \mu\text{m}$ emission with radius; we will offer

a theoretical explanation of the dropoff in density with a more detailed model in Section 5.

Note that while we include a central hole in the dust distribution, the model does not reproduce the strength of $24\ \mu\text{m}$ emission towards the center of N49. This may perhaps be the result of some non-sphericity in the N49 bubble, resulting in less dust along the line of sight to the central source. Or, as we suggest later for other reasons, if the dusty medium inside the WBB is clumpy, that could result in an enhanced contrast between the central hole and shell of $24\ \mu\text{m}$ emission for some lines of sight (K. Wood 2009, private communication).

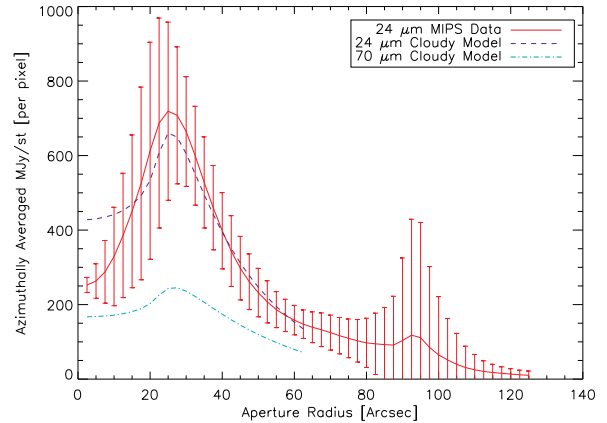


Figure 1. The best-fit model for $24\ \mu\text{m}$ emission within the wind-blown bubble, using an ISM dust-grain distribution with the photoionization model parameters given in Table 1. The solid line shows the azimuthally averaged flux from *Spitzer* MIPS data, while the dashed line shows the photoionization results, using the same azimuthal averaging. The error bars show the 1σ variation in the flux around the averaged aperture.

This fit shows that it is possible, with an ISM-like dust distribution and with a plausible gas density & temperature, to reproduce the $24\ \mu\text{m}$ observations. But is an ISM-like dust distribution the only one that is consistent? We can check further whether our dust distribution is reasonable by comparing to observations at other wavelengths; in particular, *Spitzer* MIPS data at $70\ \mu\text{m}$ taken simultaneously with the $24\ \mu\text{m}$ observations. If small dust grains are preferentially destroyed, then N49 would have a dust-grain distribution weighted towards large-dust grains; requiring such large grains to reproduce the $24\ \mu\text{m}$ emission would require a large increase in the total number of large grains; that increase would produce a greater amount of $70\ \mu\text{m}$ emission relative to $24\ \mu\text{m}$ emission than for a normal ISM-like dust distribution.

It is important to point out, however, that the observed $70\ \mu\text{m}$ emission has many contributions: it is a function of the total starlight intensity in the vicinity of N49, including stars other than the central OV star, and is not due to the hot post-shock gas in the WBB, as for the $24\ \mu\text{m}$ emission. It is therefore not surprising that (as we will see) there is a significant background of $70\ \mu\text{m}$ emission observed far from the post-shocked region of N49. In addition, the currently available $70\ \mu\text{m}$ *Spitzer* images have obvious stripping artifacts (i.e., not a background matching problem), one of which runs directly through the image of the N49 bubble. However, to our knowledge, the $70\ \mu\text{m}$ data have been carefully calibrated and should provide a reasonably correct approximate upper limit to constrain the dominance of large dust grains in N49.

⁴ <http://ssc.spitzer.caltech.edu/mips/descrip.html>

So, to examine this constraint, we ask whether a grain population with only large grains could also fit the data. We test this idea by finding the best-fit model to the *Spitzer* 24 μm MIPS data with a large-grain-only population (defined as only having grains of size 0.1 to 1 μm). For this fit, the predicted 24 μm emission is very similar to that shown in Figure 1: the best-fit initial radius for this model is $\log(r_{\text{inner}}/\text{cm}) = 18.3$ and $\langle n_{\text{dusty gas}}(r_{\text{inner}}) \rangle = 17.4 \text{ cm}^{-3}$. Most importantly, though, to fit the 24 μm data, the dust/gas ratio is $10^{4.8}$ times greater than the normal ISM dust-grain case, so we are clearly forced to an *extreme* case of a large-dust-grain dominated bubble to fit the 24 μm emission in a similar fashion as shown in Figure 1.

Figure 2 compares the observed 70 μm emission with the predictions from Cloudy models with a normal ISM-like dust-grain distribution (shown with the dashed line, as in Fig. 1) and the large-grains-only distribution (shown with the dot-dashed line). The WBB with large dust grains only clearly overpredicts the observed emission (by more than a factor of two at the peak of the predicted emission), whereas a WBB model with an ISM-like dust-grain distribution is, at its peak, a factor of four below the observed emission. In addition, the observed 70 μm emission peaks much further from N49's central star than the 24 μm emission, reaching a maximum very near young stars that appear to be situated on N49's rim.

Returning to the comparison of the fits, this comparison shows that, along with the extreme over-abundance of dust required to fit the 24 μm emission with a large-grain-only dust distribution, the observations seem to require a significant population of small dust grains as well. Again, we caution that the 70 μm emission contains contributions from all surrounding stellar sources, so we do not expect the Cloudy model to match the 70 μm emission, but it is clearly a valuable constraint on the dust population in N49, and other wind-blown bubbles (Watson et al., in preparation).

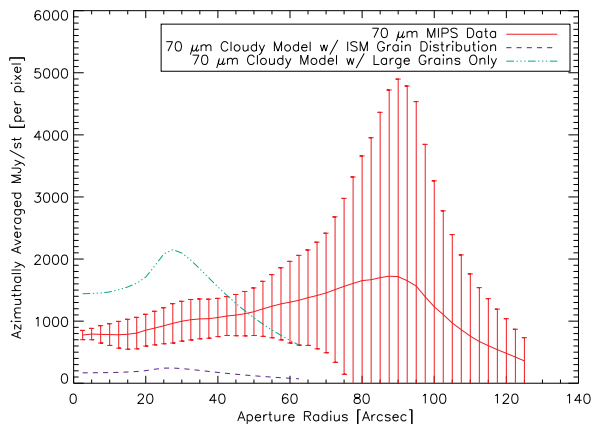


Figure 2. As in Figure 2, except that data and predictions are at 70 μm , and we include a prediction for the case where dust grains are limited to have sizes of 0.1 to 1 μm only. Such a large-grain population results in very high 70 μm flux compared to the observed flux. The error bars show the 1σ variation in the flux around the averaged aperture.

Let us now examine where the emergent 24 μm flux is coming from: is it indeed dominated by dust, and how does the dust flux compare with the stellar flux and other contributions? To examine this, we show the model continua in Figure 3. The stellar flux is shown by the solid line (which shows

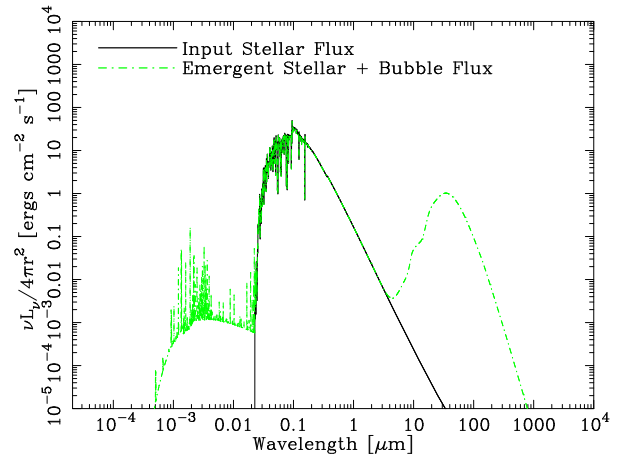


Figure 3. A comparison of the continua from the best-fit photoionization model. The solid line shows the stellar continuum that is input into Cloudy. The green, dashed line shows the full continuum emerging from the star+wind-blown bubble system. In the X-ray and UV (from 10^{-4} to 10^{-2} μm), the 3.5×10^6 K gas of the wind-blown bubble dominates, while at $\lambda \gtrsim 4 \mu\text{m}$, dust emission clearly dominates.

the input stellar flux); it is reasonably approximated with a blackbody, although stellar-wind absorption features (around $\sim 0.1 \mu\text{m}$) are present. The green, dashed line shows the flux that emerges from the dusty, wind-blown bubble and star, together. At wavelengths from 10^{-4} to 10^{-2} μm (in the UV to X-ray regime of approximately 1 to 100 \AA), the flux is dominated by the hot wind-shocked gas in the bubble, where we have set $T = 3.5 \times 10^6$ K. On the other side of the stellar continuum, at long wavelengths of $\sim 4 \mu\text{m}$ and beyond, the dust emission dominates the continuum. In fact, one can see the 10 μm silicate feature superposed on the dust continuum. We have checked that no other line features contribute in this region, in our model; of the atomic lines in Cloudy, H I recombination lines in the *Spitzer* 24 μm bandpass contribute more than any other atomic lines, and they remain at a luminosity nine orders of magnitude smaller than the dust emission. In this dusty WBB, dust emission dominates in the 24 μm *Spitzer* bandpass.

For later comparison with dynamical models, an estimate is needed for the amount of dusty gas required in the wind-blown bubble to reproduce the observations. Given the parameters for the best-fit model, the total mass of dusty gas would be 4.8×10^{33} g, or approximately $2.4 M_{\odot}$. How does that compare with the mass available in the area swept up by the bubble? For the same outer radius, assuming an ambient density of 10^4 cm^{-3} , approximately 10^4 solar masses would be available. Thus, the dusty gas required is a small fraction of the gas available.

4. CAN DUST SURVIVE IN THIS ENVIRONMENT?

These observations and models present a strong case for N49 as a dusty, wind-blown bubble. However, there are a variety of processes that could either destroy or remove dust from the interior of a wind-blown bubble: sublimation, sputtering, radiative acceleration, and/or gas-dust friction. Can dust survive within N49?

We first examine the possibility of dust sublimation in Figure 4. In our Cloudy models, the graphite-grain temperatures are quite low, spanning the range of 40 to 140 K depending on position in the wind-blown bubble and on grain-size

(the silicate-grain temperatures are quite similar: the smallest silicate grains are approximately 25% cooler at the bubble innermost radius, and have temperatures within 10% of the graphite grains over most of the wind-blown bubble). For a given grain size, the variation in grain temperature is only about 50% throughout the entire bubble. Overall, the grain temperatures are much lower than the grain sublimation temperature of ~ 1500 K, so the grains are in little danger of being sublimated away. We note that, also, the dust temperatures given here are quite similar to those observed in other wind-blown bubbles (Watson et al., in preparation).

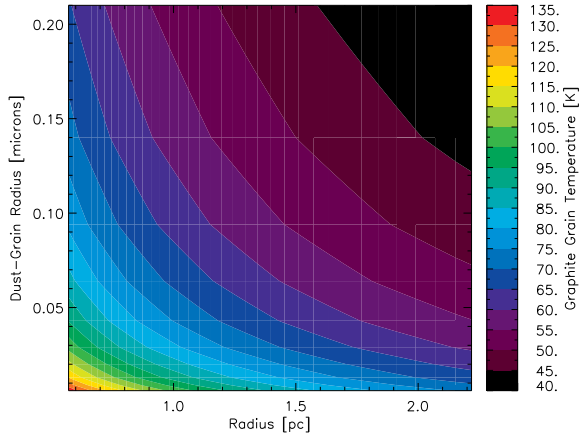


Figure 4. The graphite-grain temperature as a function of radius in the wind-blown bubble and as a function of dust-grain size. The grain temperatures are significantly lower than the grain sublimation temperature of 1500 K, so even the smallest, hottest grains do not sublimate away.

We next test whether the grains are sputtered away by gas-grain collisions. For this, we first assume that the grains are stationary relative to the bulk motion of the post-shock gas (i.e., that the gas and dust have the same flow velocities), an approximation that we will later see is quite good, given the dust-gas coupling in the post-shock region. We calculate the sputtering rates from the formula derived by Tielens et al. (1994), and present the results in Figure 5.

The sputtering rates depend only on the size of the grain and (for the assumption that the gas and grains are well-coupled and moving at the same velocity) the temperature of the surrounding gas. We can see that for the assumed temperature of 3.5×10^6 K, the sputtering times for grains with radii less than about $0.1 \mu\text{m}$ are $\lesssim 10^6$ years, the approximate estimated age of N49 ($\sim 10^6$ yrs). We caution that these sputtering timescales should be recognized as upper limits on the sputtering time; before dust is accelerated to the gas velocity, the dust grains will suffer collisions with gas ions of greater relative velocity, and so will have a somewhat lower survival time than shown here.

Of course, this result is strongly dependent on the gas density in the post-shock region. Integrating the equations for a simple (dust free) Weaver et al. (1977) wind-blown bubble, we find that for an external density of 10^4 cm^{-3} , the bubble’s internal density is approximately 10 cm^{-3} at an age of approximately 5×10^5 years (we will discuss this model and more complicated models later in Section 5). This results in much faster sputtering than in the internal density in the Weaver et al. (1977) models, where the internal density was

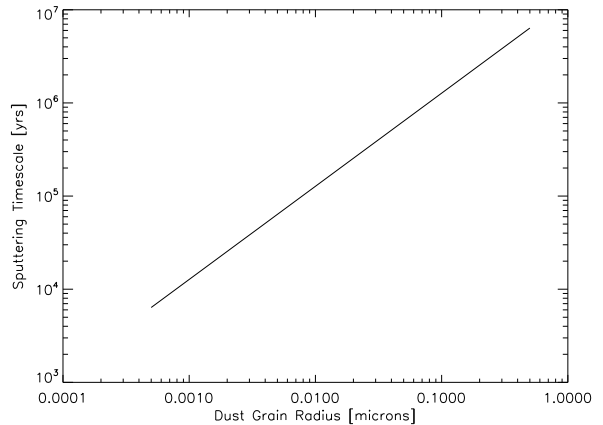


Figure 5. The sputtering rates for grains of a variety of sizes within the 3.5×10^6 K post-shock bubble of N49 for the assumed post-shock gas density of 19.1 cm^{-3} (the sputtering rate increases linearly with gas density). The sputtering times for grains are smaller than the estimated age of the N49 bubble for grains of size less than $0.1 \mu\text{m}$.

approximately 0.03 cm^{-3} , because of their lower external density of 1 cm^{-3} (at $t = 10^6$ years in their Figure 3).

We also check how quickly the grains are evacuated from the bubble by being swept up in the post-shock gas; the results of this calculation are shown in Figure 6.

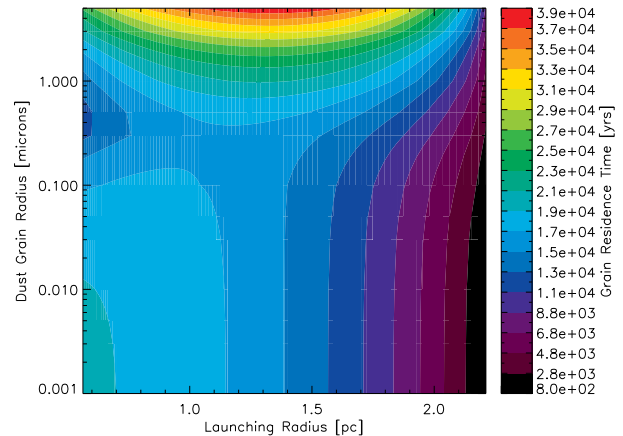


Figure 6. The residence time of dust within the wind-blown bubble, computed using the frictional force the dust grains feel because of the post-shock gas streaming past them. We calculate the time it takes each dust grain to be accelerated from its starting position (“launching radius”) to the edge of the nebula, and plot that time for a range of dust-grain sizes.

To calculate the acceleration of dust due to dust-gas friction, we make the following assumptions. First, we assume that the velocity of the post-shock gas follows the velocity law derived by Weaver et al. (1977, page 379). As mentioned previously, we assume a wind velocity of 2600 km s^{-1} . We calculate the friction between dust and gas using the results of Berruyer & Frisch (1983), and model the acceleration of the dust in the presence of that drag force and the gravitational potential of the central star (we find radiative acceleration only leads to a small drift velocity between the dust and gas that ranges between 5 and $\lesssim 15 \text{ km s}^{-1}$, depending on grain size, which is negligible compared to the $\gtrsim 500 \text{ km s}^{-1}$ velocities

of the post-shock gas and dust, as shown below). We separately derive the acceleration vs. grain size for dust at a range of initial radii within the wind-blown bubble, and then calculate how long it takes a dust grain to transit from its starting position to the edge of the nebula. This gives us the grain residence time, which is plotted for a range of launching radii and dust-grain radii in Figure 6.

As expected, the larger dust grains have greater inertia, and so take longer to be accelerated by dust-gas collisions, and have correspondingly longer residence times, but only by a factor of approximately two. Again, given the approximate age of N49 at 5×10^5 to 10^6 years, it appears that all dust would be evacuated from the bubble on timescales of order 10^4 years, much less than the bubble age. In fact, gas-grain friction would evacuate dust from the bubble on shorter timescales than the sputtering timescale; the sputtering timescale is smaller only for very small grains with sizes of order $0.001 \mu\text{m}$. So, both processes indicate a much shorter dwell time for dust than the approximate age of the bubble, although gas-grain friction is the primary mechanism of dust-grain removal for grains of all sizes.

One possible explanation for the presence of dust in this environment (that we will investigate in more detail in Section 5) is that dust grains could be the product of evaporating, colder, more dense condensations, or ‘cloudlets’, within the wind-blown bubble. Perhaps dusty cloudlets are advected into the WBB, and are then stripped away by the post-shock gas within the bubble. This process of cloudlet advection and destruction has, of course, been studied by researchers before (e.g., Cowie & McKee 1977; Pittard et al. 2001a,b; Pittard 2007) albeit not including the effects of dusty cloudlets, to our knowledge. Another possible source of dust replenishment might be debris disks of low-mass stars formed along with the O5V star in N49, which could be ejecting dust particles.

As dust emission seems to fit the observations, we continue to pursue the role of dust in cooling the bubble in the following sub-sections. We first show how the charge on dust varies within the bubble, and then what effect the dust cooling has on the bubble; we will then assemble these results into a model of N49.

4.1. Charge on Dust in the Wind-Blown Bubble

The impact of dust on the thermal balance of the dusty WBB is determined largely by the charge on the grains. In Figures 7 and 8, the average graphite grain charges are presented: in Figure 7, the average grain charge is computed over all grain sizes and over all radii (with no weighting to take into account the greater volume at larger radii, or the greater number of smaller-diameter dust particles). Figure 8 shows the average charge of grains with radii $\lesssim 0.01 \mu\text{m}$. We investigate these trends to better understand the role of dust in WBBs.

There are two trends to note in Figures 7 and 8: first, as the luminosity increases, the increased UV flux ejects more photo-electrons from the grains, pushing the grains to more positive charges. But, as the average ambient density decreases, the ambient electron density decreases, leading to fewer collisions with electrons, and resulting in more positively charged grains. Grain charge impacts both heating and cooling, which are important in our simulations: collisional heating of grains accounts for approximately 32% of the grain heating, while radiative heating of grains represents the remaining 68% of grain heating.

In Figures 7 and 8, we consider only graphite grains, but the

average charge on silicate grains is very similar to the graphite grains; the average silicate-grain charge transitions to negative values at slightly higher luminosity and lower density (by approximately 0.3 dex), compared to the average graphite grain charge, but otherwise the trends are very similar.

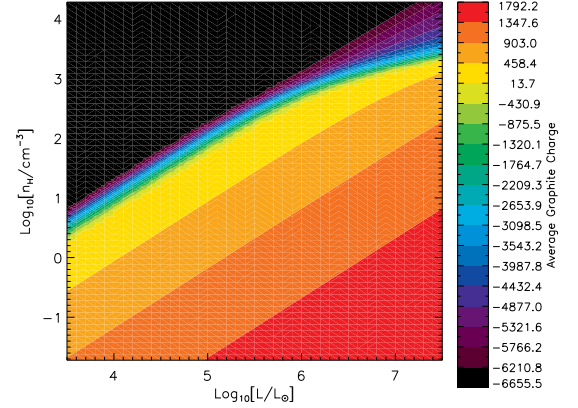


Figure 7. The average graphite dust-grain charge in our Cloudy models of the dusty wind-blown bubble. The average here is taken over all radii, and over all grain sizes, and is plotted vs. the luminosity of the central star, L , and the density of the post-shocked gas, n_H . (NB: this average is not weighted for the volume occupied by grains at each radius, or for the relative populations of grains of different sizes!) As expected, at higher luminosities photo-emission of electrons becomes an important process and the grains become positively charged; on the ordinate, meanwhile, the grain charge becomes more negative as n_e increases.

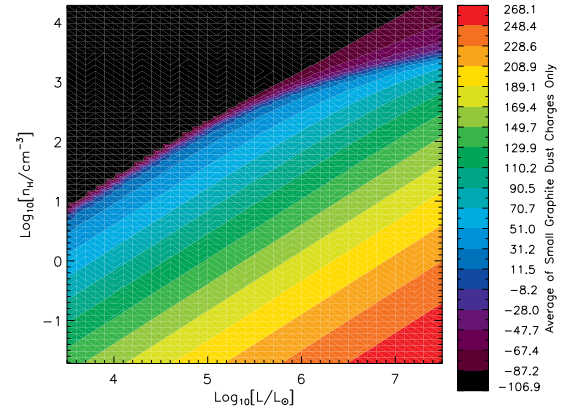


Figure 8. As in Fig. 7, but with the average taken only over the three smallest grain sizes ($a \lesssim 10^{-2} \mu\text{m}$). The same trends can be seen as in Fig. 7, but for the smaller grains, which dominate the grain distribution by number.

4.2. What is the Effect of Dust on the Wind-Blown Bubble?

If dust can survive, dust cooling will be dominant in the hot, post-shocked gas of a wind-blown bubble. This is illustrated in Figure 9, where we compare cooling curves from Cloudy where dust has not been included in the model (solid line) and where dust has been included (dashed line). We can see from Figure 9 that in the hot, post-shocked gas of the WBB (see, e.g., Freyer et al. 2006), dust cooling will be dominant for $T \gtrsim$

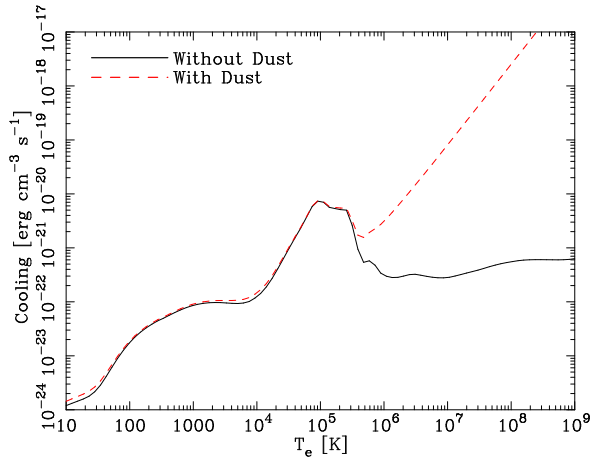


Figure 9. Gas cooling curves within the WBB for the case where dust is not included (solid line) and when ISM dust is included (dashed line); the dust-to-gas mass fraction is set to 6.3×10^{-3} , as in all of our calculations. As expected, where the atomic cooling starts to drop off near 4×10^5 K, the dust cooling starts to dominate. For the hot, post-shocked gas, if dust can survive in that region, dust will dominate the cooling.

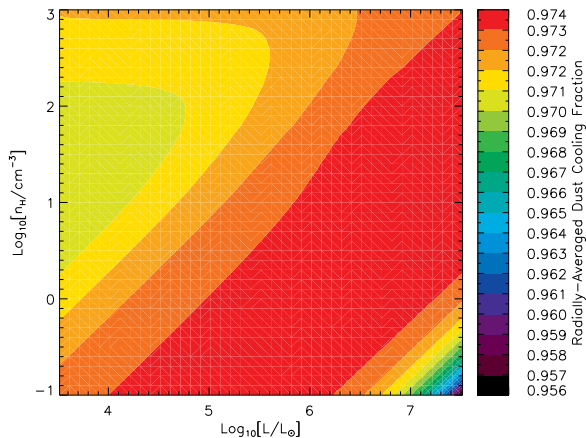


Figure 10. The fraction of cooling from dust for a range of values of central stellar luminosity and hot-gas density (the parameters for the hot gas in N49, inferred from the mass outflow rate, are at the center of this plot). The dominance of dust is evident across all of the parameter space surveyed; note the suppressed zero on the legend, at right. Only on the lower-right portion of the plot does Compton cooling start to become a factor.

5×10^5 K. We can see this for a wider range of parameters in Figure 10.

But how does dust impact the WBB dynamics? First, in considering the size of the WBB, the dust column that we find is not large enough (in the post-shocked region of the nebula) to absorb a significant fraction of the ionizing radiation; overall, dust absorbs less than 3% of the stellar flux in the energy range of 0.01 Ryd to 20 Ryd (see Fig. 11). And yet, this small amount of dust can *significantly* impact the cooling and evolution of the WBB.

We present a simplified numerical model for N49 by integrating the equations of motion for a Weaver et al. (1977) WBB and including dust cooling. For this, we use the standard equations of wind-blown bubble expansion from Weaver et al. (1977) (see, for a summary of the equations, Harper-Clark & Murray 2009), with the exception of a slightly improved cooling term in the equation for the rate of

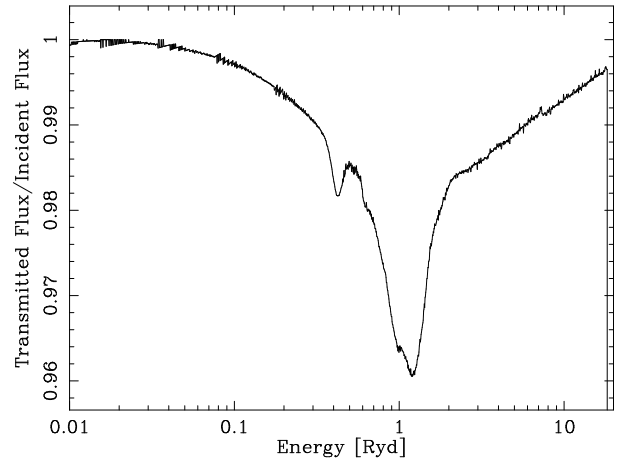


Figure 11. The ratio of stellar flux transmitted through the wind-blown bubble to the incident stellar continuum. The peaks in absorption correspond to increase in dust absorption properties at 2200 \AA (~ 0.4 Ryd) and at ~ 1 Ryd. The cutoff in the fraction at approximately 20 Ryd is due to the complete fall-off of stellar flux at that limit, so the ratio becomes ill-defined.

increase of mass inside the bubble:

$$\frac{dM_{\text{Bubble}}}{dt} = C_1 T_{\text{Bubble}}^{5/2} R_{\text{Bubble}}^2 (R_{\text{Bubble}} - R_{\text{Wind}})^{-1} - C_2 \frac{\mu L_{\text{Bubble}}}{k T_{\text{Bubble}}} \quad (1)$$

where, instead of using $T_{\text{Bubble}} = 2 \times 10^5$ K as assumed in Weaver et al. (1977), we use the temperature in the wind-blown bubble at each time-step, and calculate the luminosity, L_b , using the dust-dominated (at high T) cooling curve from Cloudy (note that this equation assumes that the mass-loading from evaporation of the surrounding dense shell is dominant; we will examine this assumption at the end of Section 5). To start with a simple model, and to isolate the effects of dust alone, we assume that dust is added at the same rate as gas to the WBB, so that dust is kept at a constant dust-mass-to-gas-mass ratio.

The result of this calculation is shown⁵ in Figure 12. We have checked the calculation by duplicating the results in Weaver et al. (1977) in the dust-free case. Note also the transition at $t \sim 10^2$ years, in our models, from dust-free initial conditions to the dusty WBB dynamics; the initial radiation losses are high enough that M_{bubble} ceases to grow in mass, and for these times, we set $dM_{\text{bubble}}/dt = 0$.

Figure 13 shows the same model, with the same initial parameters, except that dust is not included in this model. One can see that (as in Weaver et al. 1977), the luminosity increases with time, in contrast to the model with dust cooling presented in Figure 12. In fact, the dusty WBB has a luminosity at $t = 10^4$ years that is approximately a factor of six higher than the luminosity of the dust-free WBB. As a result, by an age of 10^7 years, if the central star lives that long, the energy contained within the dusty WBB is approximately a factor of eight less than the energy in the dust-free bubble.

The temperature indicated by the dynamical model of this dusty wind-blown bubble is approximately 3.5×10^6 K at an age of 10^5 years; this temperature only slightly decreases over time to $\sim 3 \times 10^6$ K at 10^6 years. This model was therefore used to set the fiducial temperature and density that we have

⁵ We note that this includes non-radiative cooling of electrons due to the electric potential of the dust grains, and as such, we will overestimate the observed luminosity of the bubble.

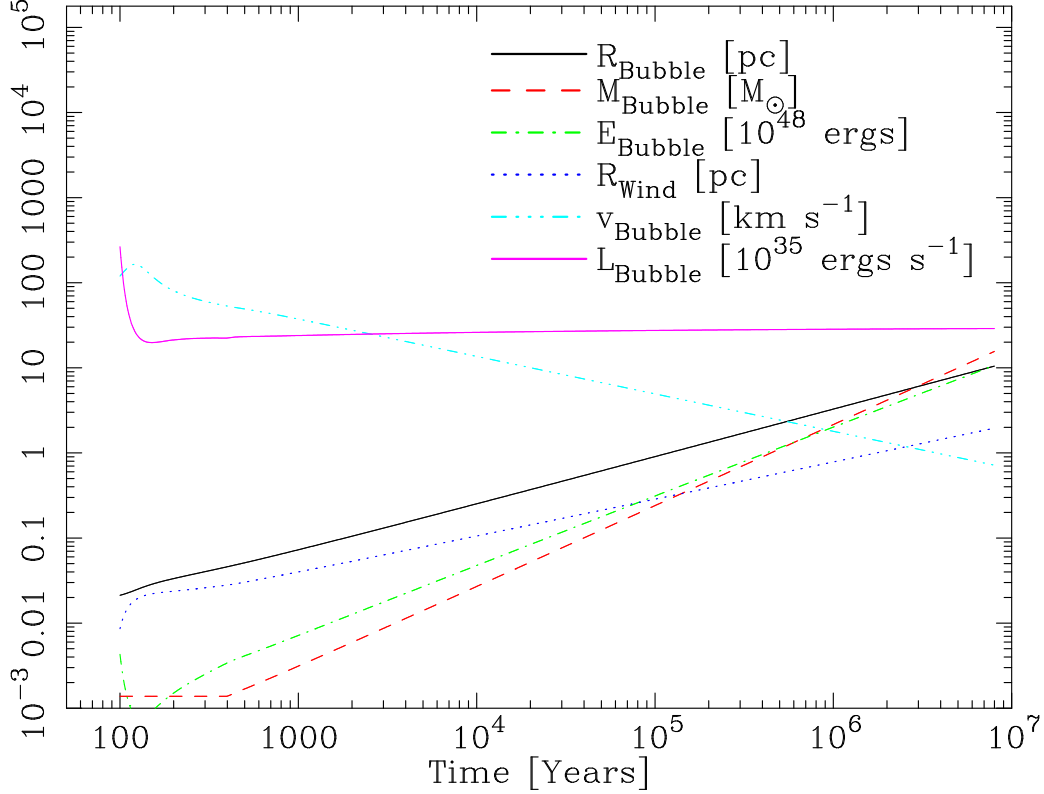


Figure 12. Analytic calculation of the growth of a wind-blown bubble with dust cooling included. In the legend, R_{Bubble} refers to the outermost radius of the wind-blown bubble (R_{Bubble} is labeled R_2 in Weaver et al.); in N49, this is identified with the innermost radius of the PAH emission. M_{Bubble} shows the amount of mass that has been evaporated from the ISM shock and subsumed into the post-shocked gas (M_{Bubble} is M_b in Weaver et al.). E_{Bubble} is the total energy in hot gas within the post-shocked gas, R_{Wind} is the radius of the wind-dominated, dust-free region inside the post-shocked gas (these are E_b and R_1 in Weaver et al., respectively). v_{Bubble} is the velocity of the outermost shock of the bubble, and L_{Bubble} is the total luminosity (including dust emission and also including non-radiative cooling of electrons due to dust-grain charge) from the post-shocked gas (corresponding to V_2 and L_b in Weaver et al., respectively). The upturns in luminosity, energy density, and mass in the bubble at $t=200$ years are the transitions from Weaver et al. (1977) initial conditions to our dynamical model that includes dust cooling. The near-constant luminosity is the result of the increasing size of the bubble compensating for both the slowly decreasing density in the bubble and the slow drop in cooling as the temperature decreases (this calculation assumes a constant temperature throughout the WBB at any given time, which slowly decreases over time).

used in earlier sections of the paper, in order to be relatively self-consistent with the parameters used. (Earlier models of ours assumed a temperature of $T \sim 10^7$ K as in Freyer et al. (2003); as mentioned earlier, that different temperature does not affect our results significantly.)

It is important to note that, in this model, the gas temperature inside the dusty WBB is approximately the same as the dust-free WBB for ages $\gtrsim 10^3$ years. This is surprising, since dust is such a strong coolant. However, this coolant is most important at early times, when the WBB temperature is $\sim 10^7$ K; at such high temperatures, the dust cooling rate is much higher than the gas-derived cooling rate. So, in the early evolution of the WBB, when dust is introduced in the model, it is indeed a strong coolant: the resultant WBB luminosity is very high, and the temperature and energy in the bubble drop sharply. In the Weaver et al. model, such a high luminosity implies a lower energy input to the outer shell of the WBB, and therefore a decrease in the evaporated mass-flux from that shell into the bubble. This decrease in mass flux and the energy lost due to radiation in this $\sim 10^7$ K phase roughly track each other, and so the overall temperature in the bubble does not change greatly. Therefore, in this model, the dust impacts the growth of the bubble (its size and mass), but does not greatly affect the temperature.

This WBB model also approximately reproduces other features of N49. The inner radius of the bubble reaches 0.5 pc at an age of 3×10^5 years, and at the same time has an outer radius of approximately 1.8 pc, close to the 2.2 pc that we derive from observations. The expansion velocity of the bubble is approximately 3 km s^{-1} at that same age.

But how can dust exist continuously in the post-shocked bubble? We consider that possibility in the next section.

5. A PROPOSED MODEL FOR N49

Our photoionization and (as yet, quite simplified) dynamical modeling of N49 shows the possible importance of dust on the bubble. However, as shown in earlier sections, due to the relatively small timescale of dust advection in the post-shock bubble, that dust must be somehow resupplied. As mentioned in Section 4, we hypothesize that small, dense ISM ‘cloudlets’ have been over-run by the ionization front of the bubble (see Figure 14). When these cloudlets interact with the shocked wind, they are gradually disrupted, releasing their dust and gas into the post-shocked wind. The dust grains from these cloudlets then yield the $24 \mu\text{m}$ emission that is observed. The dust adds to the radiative cooling of the post-shock gas, and decreases the energy density in the bubble over time (\dot{E}_p in Fig. 14) relative to dust-free wind-blown bubbles.

We note that, while the presence and importance of dust within wind-blown nebula is a relatively new idea, the presence of substructure, or ‘clumps’, within nebulae has been inferred in a variety of other observations, from early studies of line ratios in the Orion Nebula (Osterbrock & Flather 1959) to the impact of clumps on observations of the radio-continuum spectral slope⁶ (Cassinelli & Hartmann 1977; Ignace & Churchwell 2004). Extensive theoretical work has already been done on the inclusion of clumps and the resulting mass-loading (see Pittard et al. 2001a,b); for a review, see Pittard (2007) and references therein.

To further check this picture, we estimate how quickly these cloudlets are destroyed within the WBB, and check whether

such resupply is consistent with observations and the model. To examine this, we calculated the mass deposition from the cloudlets into the WBB, where the cloudlets are stripped away by both ablation and evaporation due to the fast-moving, hot post-shocked wind that surrounds them. [The ram pressure and thermal pressure of the post-shocked wind would, together, suppress photoevaporation of the clouds; in addition, even if photoevaporation were present and not suppressed, it would result in mass-loss rates of order the ablation and conduction rates, so would not significantly change our estimates, especially given other uncertainties (Pittard 2007).] To estimate the effects of these processes, we used the approximate equations of Pittard (2007). First, for ablation, where the external flow is subsonic, we calculate:

$$\dot{M}_{\text{ablation}} \approx \mathcal{M}^{4/3} (M_c c_c)^{2/3} (\rho v)^{1/3} \text{ g s}^{-1}, \quad (2)$$

where \mathcal{M} is the Mach number of the post-shocked wind flow, M_c is the mass of the cloudlet, c_c is the speed of sound within the cloudlet, ρ is the mass density of the post-shocked wind, and v is the velocity of the post-shocked wind. For a supersonic flow,

$$\dot{M}_{\text{ablation}} \approx (M_c c_c)^{2/3} (\rho v)^{1/3} \text{ g s}^{-1}. \quad (3)$$

Meanwhile, the mass loss to conduction is given by

$$\dot{M}_{\text{conduction}} \approx 2.75 \times 10^{19} \omega r_{c,\text{pc}} T_6^{5/2} \text{ g s}^{-1} \quad (4)$$

where $\omega = 1$ gives the limit of classical evaporation (which we adopt here), T_6 is the temperature in the wind-blown bubble in units of 10^6 K, and $r_{c,\text{pc}}$ is the radius of the cloudlet in parsecs (again, see Pittard 2007).

To use these equations, we take the density within the bubble from our simple dynamical model (shown in Fig. 12) at $t = 5 \times 10^5$ years, and use the approximation for v within the wind-blown bubble from page 379 of Weaver et al. (1977):

$$v \sim \frac{v_{\text{wind}}}{4} \left(\frac{15}{16} \right)^{3/2} \frac{R_{\text{wind}}^2}{r^2}, \quad (5)$$

again using the wind velocity, post-shocked wind temperature, and bubble radius from our dynamical model. We then check whether there exist reasonable cloud parameters (M_c , c_c , and $r_{c,\text{pc}}$) that would yield the required mass-outflow rate given the above ablation and conduction mass-loss estimates, and which would have enough mass to survive for 5×10^5 years.

Specifically, we require that the cloudlets need to resupply the observed dusty-gas mass ($\sim 2.5 M_\odot$ of gas) every 10^4 years (the shortest timescale for dust sublimation and evacuation from the bubble). If the wind-blown bubble is $\sim 5 \times 10^5$ yrs old, then $125 M_\odot$ of dusty gas is required to be resupplied to the bubble interior in that time. The average mass loss rate is then, of course, $2.5 \times 10^{-4} M_\odot \text{ yr}^{-1}$ from all of the cloudlets embedded in the post-shock gas. Can cloudlet ablation or conduction (or both together?) in the post-shock region match that rate, and with a reasonable number of clouds?

Looking at Equations 2 through 4, the conductive and ablative mass-loss rates depend not only on the number of cloudlets, but also the cloudlet density, radius, and temperature. With these unknown parameters, we cannot claim a unique solution. Of all of those parameters, we can only approximately set the density within the cloudlets, choosing

⁶ The radio-continuum spectral slope can also be modified by the power-law drop-off of density with radius (Panagia & Felli 1975; Olmon 1975)

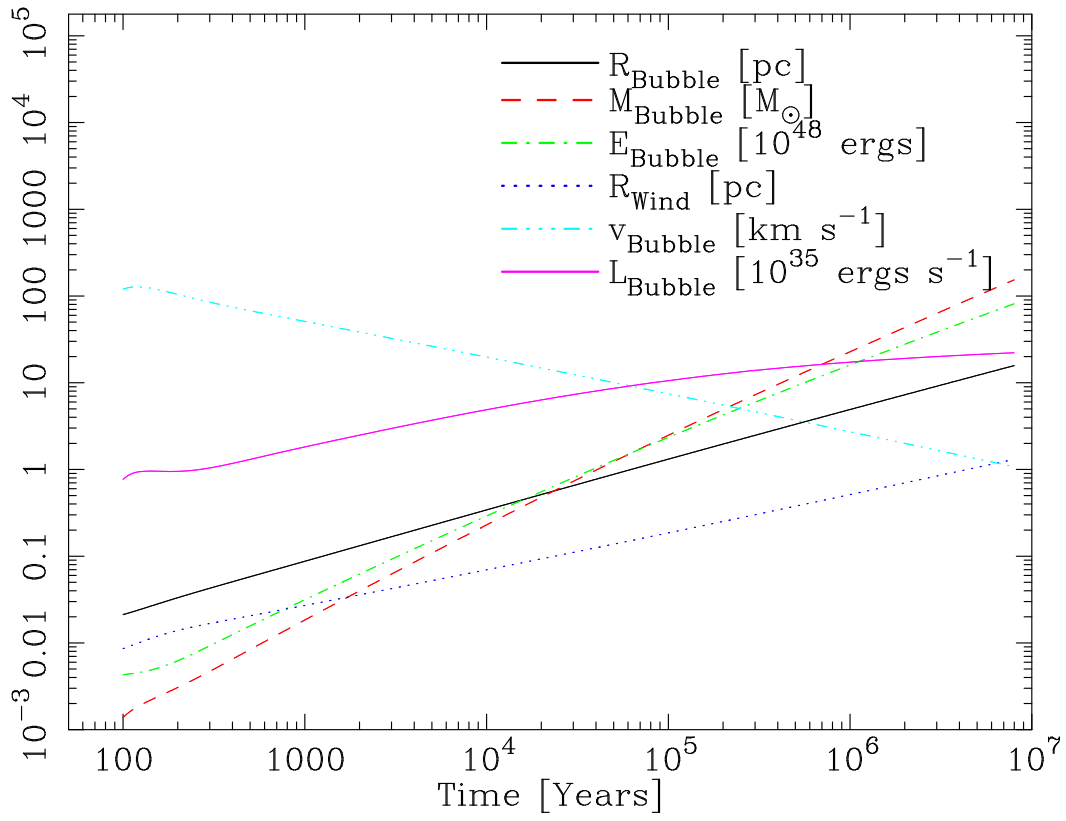


Figure 13. As in Figure 12 but without dust cooling included.

$n_{\text{cloudlet}} = 10^5 \text{ cm}^{-3}$ as an approximate high-density component of the external medium. After a search of parameter space, we find that requiring these clouds to lose mass at a rate of $\sim 2.5 \times 10^{-4} M_{\odot} \text{ yr}^{-1}$ can be satisfied if the clouds have a radius of approximately 0.05 pc or $\sim 10^4$ AU and a cloud temperature of about $T \sim 100$ K. Interestingly, the size of these clouds is in the range of clouds observed in De Marco et al. (2006) and Koenig et al. (2008). The mass of each individual cloud is approximately $1.3 M_{\odot}$; the mass of dusty-gas within the bubble could be replenished by a few hundred of these kinds of clouds, spread throughout the wind-blown bubble, occupying only approximately 0.5% of the volume of N49.

With these parameters, cloud ablation dominates for most of the interior of the wind-blown bubble, whereas thermal evaporation due to conduction is important only for $R \gtrsim 1.5$ pc. This transition occurs because the velocity of the post-shocked gas decreases with radius (see Eq. 5, from Weaver et al. 1977) as r^{-2} , so that ablation becomes less important with radius in the wind-blown bubble. If ablation were the only important cloud destruction process, $\dot{M}_{\text{ablation}} \propto \mathcal{M}^{4/3} v^{1/3} = (v/c_{s,\text{ext}})^{4/3} v^{1/3} \propto v^{5/3}$ (where $c_{s,\text{ext}}$ is the sound speed in the external medium), and since $v \propto r^{-2}$, we would expect $\dot{M}_{\text{ablation}}$ and the resultant dust density to scale as $r^{-10/3}$ or approximately as r^{-3} . Conduction at larger radius adds another mass-loss term, however, so we would expect the dust distribution to drop off somewhat more slowly than r^{-3} . Also, dust-gas friction will push dust to larger radii within the bubble and would tend to flatten the radial distribution of dust. So, in the end, our model's assumed dust distribution of r^{-2} is not unreasonable. Much more work is needed to try to understand the details of this process however; we have aimed merely to physically justify the assumptions of our model and to try to build a reasonably self-consistent picture. It must be noted that cloud destruction in this environment is a complicated and non-linear process, and so the above expressions are only rough estimates of this process; the rate of cloud ablation would certainly change over time as gas and dust are added to the post-shocked gas, for instance.

One difficulty with the above simple explanation for dust-loading that points to further work is the amount of dusty gas that is added to the pressurized interior of the bubble. We have employed the models of Weaver et al. (1977), but with $125 M_{\odot}$ of dense cloudlets added to the bubble over 10^5 years, the mass in the cloudlets will overwhelm the addition of mass via thermal conduction from the outer shell (assumed to be the main component of mass addition in Weaver et al. 1977), dominate mass addition to the interior of the bubble, and cool the bubble interior and impact its dynamics (see, e.g., Arthur et al. 1993; Pittard et al. 2001b; Nazé et al. 2002). The necessity for so much added gas mass could point to improvements that must be made to our initial assumptions and calculations: perhaps such dense cloudlets have larger dust grains than we have assumed that are not destroyed as quickly (but that yield smaller dust grains via slow sputtering), or perhaps normal-sized ISM grains last longer than the above estimates of dust destruction indicate. The possibility of longer-lived grains could actually be related to the added gas mass, which could cool the bubble interior and impacts the gas dynamics within the hot bubble; both of these processes may slow the destruction of grains, although, possibly countering this, an increased density within the bubble would (by itself) increase dust sublimation rates proportionately.

Regardless, it is clear that the presence of dust and of cloudlets point to the necessity of new and more detailed models of wind-blown bubbles: when we run simple models with the above mass-injection rates (from cloudlets), we find that the bubble quickly cools. In fact, even with mass-injection rates an order of magnitude lower than those postulated above ($2.5 \times 10^{-5} M_{\odot} \text{ yr}^{-1}$), the hot-pressure bubble cools after only a few hundred years. With mass input rates of $2.5 \times 10^{-6} M_{\odot} \text{ yr}^{-1}$, the bubble expands for millions of years without cooling. This could indicate a critical upper limit for the addition of mass in cloudlets. We stress again, however, that the above estimates are very simple and point the way to necessary improvements of the basic models of wind-blown bubble expansion, possibly along the lines of models such as those of Hanami & Sakashita (1987) and Pittard (2007), or the models of cloudlets within supernova remnants, as in Pittard et al. (2003).

6. CONCLUSIONS

We were intrigued by the possibility of dust within the wind-blown bubble 'N49' (Watson et al. 2008). Our goal was to explain the present observations with dust, and to try to understand how dust may survive within that environment. In this paper, we found that both the processes of dust-gas friction and sputtering of small dust grains can lead to the evacuation of dust grains from WBBs on relatively short timescales of approximately 10^4 years. We also found, though, that if dust is present, it has a very significant effect on the structure of the wind-blown bubble: decreasing the energy within the bubble due to dust cooling, and therefore decreasing the size of the bubble relative to dust-free bubbles. However, in order for dust to be present in N49 today, that dust must be replenished; we hypothesize that high-density cloudlets ($n_c \sim 10^5 \text{ cm}^{-3}$) can be overrun and subsumed by the wind-blown bubble. Those cloudlets are then gradually destroyed by ablation and evaporation in the post-shock wind in the bubble, but on timescales long enough that the cloudlets would continue to supply the required density of dust to N49 over at least 5×10^5 years. Such substructure has already been suggested by other researchers (e.g., Osterbrock & Flather 1959; Pittard 2007); what is new here is the consideration of dust. We caution that the dust may be supplied by other processes, too; for instance, the ejection of dust-grains from the debris disks of nearby low-mass Young Stellar Objects might also be important.

This model has several implications. First, the external density around N49 must be fairly high to support high-density clouds ($n_c \sim 10^5 \text{ cm}^{-3}$); our dynamical model also assumes $n_{\text{external}} \sim 10^4 \text{ cm}^{-3}$ in the external medium. This should be tested by constraining the density through ammonia observations (Cyganowski et al., in preparation). Also, as dusty bubbles age, if the cloudlet density is constant with radius within the bubble, dust should gradually be evaporated from the inside out, such that there should be wind-blown bubbles with only an outer-rim of $24 \mu\text{m}$ emission; this could be tested by comparing free-free and $24 \mu\text{m}$ observations of WBBs. Finally, a similar structure of $24 \mu\text{m}$ emission should be visible in other wind-blown bubbles; as long the bubble is young enough (ages of less than 10^6 years for the cloud parameters outlined herein) that it has not destroyed all of the dusty cloudlets, similar $24 \mu\text{m}$ emission should be seen; there are hints of this already (C. Watson, personal communication). Finally, the large amount of mass-loading that appears

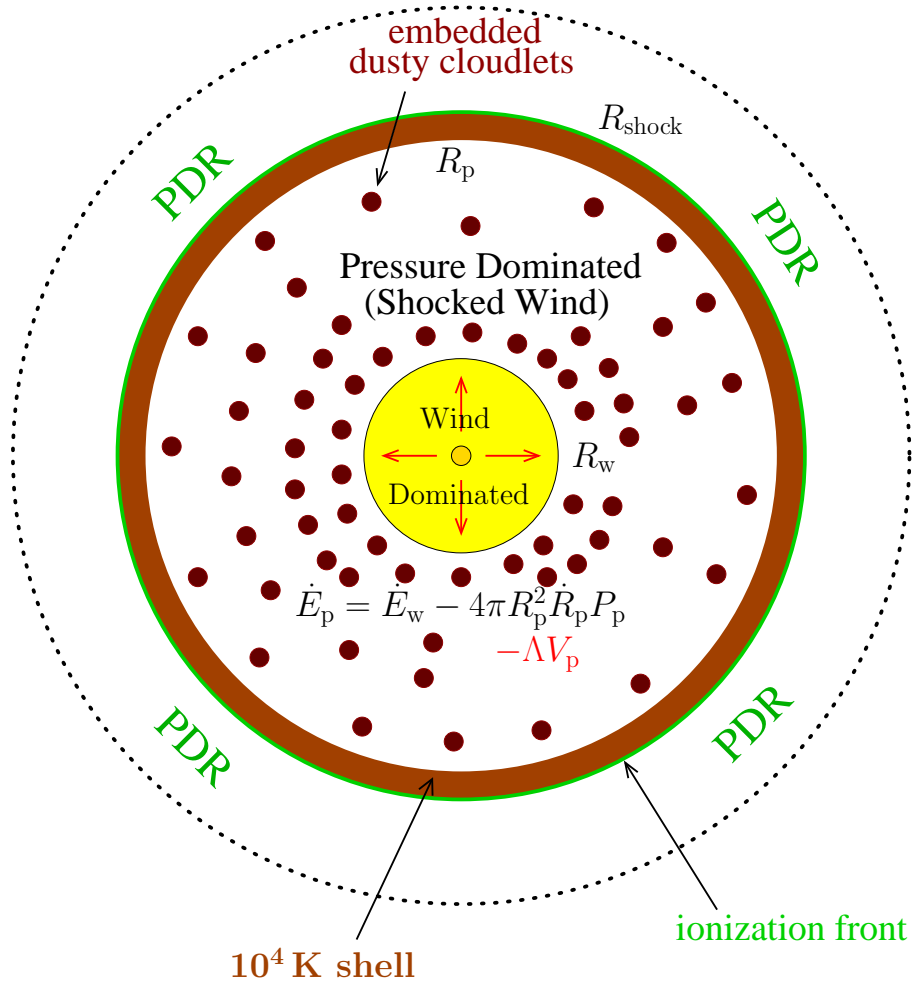


Figure 14. Our schematic of the dusty, wind-blown bubble of N49. The stellar wind has completely evacuated the central region of dust, leaving a dust-free, “wind dominated” zone of radius R_w in the center. We identify the observed central dip in azimuthally-averaged $24 \mu\text{m}$ emission in N49 with this wind-dominated region. Dust is driven from the post-shock gas by dust-gas friction and destroyed by sputtering on timescales about at least an order of magnitude less than the age of the wind-blown bubble; therefore, to resupply dust within the bubble, we hypothesize that small cloudlets are over-run by the expanding bubble, and slowly destroyed by heat conduction and ablation.

to be necessary to maintain dust in the WBB may lead to large amounts of cooling and a short lifetime for the Weaver et al. (1977) pressure-driven phase.

This work was supported by NSF AST-0808119, NASA/*Spitzer* Grant 1317498, NSF AST-0507367, NSF AST-0907837 and NSF PHY-0215581 & NSF PHY-0821899 (to the Center for Magnetic Self-Organization in Laboratory and Astrophysical Plasmas). This research has made use of NASA's Astrophysics Data System. The authors also wish to thank Gary Ferland, Peter van Hoof, and all of their collaborators for their work on the photoionization code Cloudy. The authors thank Barb Whitney, Kenny Wood, and Ellen Zweibel for helpful conversations; many thanks also to Marilyn Meade for supplying MIPS images "to order." Finally, we thank the referee for their time and effort in reviewing the paper and asking detailed, insightful questions.

REFERENCES

- Arthur, S. J. 2007, *Wind-Blown Bubbles around Evolved Stars*, ed. Hartquist, T. W., Pittard, J. M., & Falle, S. A. E. G., 183–+
- Arthur, S. J., Dyson, J. E., & Hartquist, T. W. 1993, *MNRAS*, 261, 425
- Arthur, S. J., Henney, W. J., & Dyson, J. E. 1996, *A&A*, 313, 897
- Benjamin, R. A. et al. 2003, *PASP*, 115, 953, arXiv:astro-ph/0306274
- Berruyer, N., & Frisch, H. 1983, *A&A*, 126, 269
- Carey, S. J. et al. 2009, *PASP*, 121, 76
- Cassinelli, J. P., & Hartmann, L. 1977, *ApJ*, 212, 488
- Castor, J., McCray, R., & Weaver, R. 1975, *ApJ*, 200, L107
- Chu, Y. 2003, in *IAU Symposium*, Vol. 212, *A Massive Star Odyssey: From Main Sequence to Supernova*, ed. K. van der Hucht, A. Herrero, & C. Esteban, 585–+
- Chu, Y. 2008, in *IAU Symposium*, Vol. 250, *IAU Symposium*, ed. F. Bresolin, P. A. Crowther, & J. Puls, 341–354
- Chu, Y. H., & Lasker, B. M. 1980, *PASP*, 92, 730
- Churchwell, E. et al. 2009, *PASP*, 121, 213
- . 2006, *ApJ*, 649, 759
- Cowie, L. L., & McKee, C. F. 1977, *ApJ*, 211, 135
- De Marco, O., O'Dell, C. R., Gelfond, P., Rubin, R. H., & Glover, S. C. O. 2006, *AJ*, 131, 2580, arXiv:astro-ph/0602545
- Deharveng, L., Zavagno, A., & Caplan, J. 2005, *A&A*, 433, 565, arXiv:astro-ph/0412602
- Dyson, J. E. 1973, *A&A*, 23, 381
- Falle, S. A. E. G. 1975, *A&A*, 43, 323
- Ferland, G. J., Korista, K. T., Verner, D. A., Ferguson, J. W., Kingdon, J. B., & Verner, E. M. 1998, *PASP*, 110, 761
- Freyer, T., Hensler, G., & Yorke, H. W. 2003, *ApJ*, 594, 888, arXiv:astro-ph/0306541
- . 2006, *ApJ*, 638, 262, arXiv:astro-ph/0512110
- Garcia-Segura, G., & Mac Low, M. 1995, *ApJ*, 455, 145
- Garcia-Segura, G., Mac Low, M., & Langer, N. 1996, *A&A*, 305, 229
- Hanami, H., & Sakashita, S. 1987, *A&A*, 181, 343
- Harper-Clark, E., & Murray, N. 2009, *ApJ*, 693, 1696, arXiv:0812.2906
- Hartquist, T. W., Dyson, J. E., Pettini, M., & Smith, L. J. 1986, *MNRAS*, 221, 715
- Helfand, D. J., Becker, R. H., White, R. L., Fallon, A., & Tuttle, S. 2006, *AJ*, 131, 2525
- Hensler, G. 2008, in *IAU Symposium*, Vol. 252, *IAU Symposium*, ed. L. Deng & K. L. Chan, 309–315
- Hillier, D. J. 2009, in *American Institute of Physics Conference Series*, Vol. 1171, *American Institute of Physics Conference Series*, ed. I. Hubeny, J. M. Stone, K. MacGregor, & K. Werner, 111–122
- Ignace, R., & Churchwell, E. 2004, *ApJ*, 610, 351, arXiv:astro-ph/0403689
- Johnson, H. M., & Hogg, D. E. 1965, *ApJ*, 142, 1033
- Koenig, X. P., Allen, L. E., Kenyon, S. J., Su, K. Y. L., & Balog, Z. 2008, *ApJ*, 687, L37, arXiv:0809.1993
- Martins, F., Schaerer, D., & Hillier, D. J. 2005, *A&A*, 436, 1049, arXiv:astro-ph/0503346
- Mathews, W. G. 1966, *ApJ*, 144, 206
- Mathis, J. S., Rimpl, W., & Nordsieck, K. H. 1977, *ApJ*, 217, 425
- Morisset, C. 2006, in *IAU Symposium*, Vol. 234, *Planetary Nebulae in our Galaxy and Beyond*, ed. M. J. Barlow & R. H. Méndez, 467–468
- Nazé, Y., Chu, Y., Guerrero, M. A., Oey, M. S., Gruendl, R. A., & Smith, R. C. 2002, *AJ*, 124, 3325, arXiv:astro-ph/0208430
- Nazé, Y., Chu, Y., Points, S. D., Danforth, C. W., Rosado, M., & Chen, C. 2001, *AJ*, 122, 921, arXiv:astro-ph/0104420
- Olson, F. M. 1975, *A&A*, 39, 217
- Osterbrock, D., & Flather, E. 1959, *ApJ*, 129, 26
- Panagia, N., & Felli, M. 1975, *A&A*, 39, 1
- Pasquali, A., Nota, A., Smith, L. J., Akiyama, S., Messineo, M., & Clampin, M. 2002, *AJ*, 124, 1625, arXiv:astro-ph/0207613
- Pauldrach, A. W. A., Hoffmann, T. L., & Lennon, M. 2001, *A&A*, 375, 161
- Pikel'ner, S. B. 1968, *Astrophys. Lett.*, 2, 97
- Pittard, J. M. 2007, *Mass-Loaded Flows (Diffuse Matter from Star Forming Regions to Active Galaxies)*, 245–+
- Pittard, J. M., Arthur, S. J., Dyson, J. E., Falle, S. A. E. G., Hartquist, T. W., Knight, M. I., & Pexston, M. 2003, *A&A*, 401, 1027, arXiv:astro-ph/0303258
- Pittard, J. M., Dyson, J. E., & Hartquist, T. W. 2001a, *A&A*, 367, 1000, arXiv:astro-ph/0012434
- Pittard, J. M., Hartquist, T. W., & Dyson, J. E. 2001b, *A&A*, 373, 1043, arXiv:astro-ph/0107102
- Rieke, G. H. et al. 2004, *ApJS*, 154, 25
- Smith, L. F. 1967, *AJ*, 72, 829
- Tielens, A. G. G. M., McKee, C. F., Seab, C. G., & Hollenbach, D. J. 1994, *ApJ*, 431, 321
- van Hoof, P. A. M., Weingartner, J. C., Martin, P. G., Volk, K., & Ferland, G. J. 2004, *MNRAS*, 350, 1330, arXiv:astro-ph/0402381
- Vasquez, J., Cappa, C. E., & Pineault, S. 2009, *MNRAS*, 395, 2045, arXiv:0811.3349
- Vink, J. S., de Koter, A., & Lamers, H. J. G. L. M. 2001, *A&A*, 369, 574, arXiv:astro-ph/0101509
- Watson, C. et al. 2008, *ApJ*, 681, 1341, arXiv:0806.0609
- Weaver, R., McCray, R., Castor, J., Shapiro, P., & Moore, R. 1977, *ApJ*, 218, 377
- Werner, M. W. et al. 2004, *ApJS*, 154, 1, arXiv:astro-ph/0406223
- Zhekov, S. A., & Myasnikov, A. V. 2000, *Ap&SS*, 274, 243